

Forecast Constraints on Inflation from Combined CMB and Gravitational Wave Direct Detection Experiments

Sachiko Kuroyanagi,^{1,*} Christopher Gordon,² Joseph Silk,^{2,3} and Naoshi Sugiyama^{1,4}

¹*Department of Physics, Nagoya University, Chikusa, Nagoya 464-8602, Japan*

²*Astrophysics Department, University of Oxford, Denys Wilkinson Building, Keble Road, Oxford OX1 3RH, UK*

³*Institut d' Astrophysique, 98bis Boulevard Arago, Paris 75014, France*

⁴*Institute for Physics and Mathematics of the Universe, University of Tokyo, 5-1-5 Kashiwa-no-ha, Kashiwa City, Chiba 277-8582, Japan*

We study how direct detection of the inflationary gravitational wave background constrains inflationary parameters and complements CMB polarization measurements. The error ellipsoids calculated using the Fisher information matrix approach with Planck and the direct detection experiment, Big Bang Observer (BBO), show different directions of parameter degeneracy, and the degeneracy is broken when they are combined. For a slow-roll parameterization, we show that BBO could significantly improve the constraints on the tensor-to-scalar ratio compared with Planck alone. We also look at a quadratic and a natural inflation model. In both cases, if the temperature of reheating is also treated as a free parameter, then the addition of BBO can significantly improve the error bars. In the case of natural inflation, we find that the addition of BBO could even partially improve the error bars of a cosmic variance-limited CMB experiment.

PACS numbers: 98.80.Es, 98.80.Cq, 04.30.-w

I. INTRODUCTION

Inflation [1–3], which is widely believed to have taken place in the very early universe, generically predicts the existence of tensor mode perturbations originating from quantum fluctuation [4–6]. Since inflation predicts an almost scale-invariant spectrum, the tensor mode perturbations are considered to exist as a gravitational wave background over a wide range of frequencies. Because of their weakness of interaction with matter and their linearity, they are expected to remain uncontaminated even at higher frequencies, whereas the scalar mode perturbations become nonlinear and it might seem difficult to recover information about its spectrum on smaller scales. Therefore the gravitational wave background possesses the potential to enable us to reconstruct the primordial spectrum over a wider range of scales. This helps us learn more about the inflation potential since the amplitude of the spectrum at each scale corresponds to the height of the potential when the mode exited the horizon during inflation.

One of the ways to detect the inflationary gravitational wave background is to measure the B -mode polarization of the cosmic microwave background (CMB) induced by primordial gravitational waves [7, 8]. The ongoing satellite mission, Planck [9], is expected to detect the signature of the large-scale tensor perturbations if they are sufficiently large in amplitude. The other way of probing the gravitational wave background is to detect it directly with space-based laser interferometers such as Big Bang Observer (BBO) and DECi-hertz Interferometer Gravitational wave Observatory (DECIGO) [10, 11]. Clearly,

both approaches provide us with new information about the early universe, and help in determining inflationary parameters more accurately if they detect the gravitational wave background. It is notable that while CMB B -mode experiments measure the gravitational wave background at the present horizon scale ($\sim 10^{-18}$ Hz), direct detection experiments measure it at much smaller scales which correspond to the detector size ($\sim 0.1 - 1$ Hz). This means that these two different types of experiments could provide independent information.

In this paper, our goal is to predict how the direct detection of the gravitational wave background can complement CMB observations. The complementarity of the two observations is discussed within the slow-roll paradigm in Refs. [12–14]. While they only discuss the detectability of the gravitational wave background in direct detection experiments by connecting the amplitude of the gravitational wave background at direct detection scales with model parameters which are allowed by the current CMB constraints, we perform the Fisher matrix calculation and forecast errors on the parameters attainable in the direct detection experiments. This enables us to discuss how well inflation parameters may be determined by direct detection of the gravitational wave background and how degeneracy in parameter space may be broken when the two constraints from CMB observation and direct detection are combined.

Here, we consider the combination of the upcoming CMB satellite experiment Planck and the future satellite gravitational wave detector BBO. As long as we make the usual assumption that the equation of state is ≥ -1 during inflation, the spectrum of the gravitational wave background cannot be blue-tilted and sensitivities of ground-based experiments and the preceding space mission LISA are not enough to detect the inflationary gravitational waves. Therefore, it would be a long road

*s-kuro@a.phys.nagoya-u.ac.jp

to seek the inflationary gravitational waves, while CMB experiments are expected to detect B -mode signals in the not so distant future. One may think constraints on inflationary parameters may be improved by post-Planck CMB experiments before direct detection is achieved by BBO. For this reason, we also look at the case combined with a cosmic variance-limited experiment, which would be similar to CMB satellite missions planned for a few decades like BBO, instead of Planck.

Applying the Fisher matrix method to the specification of Planck and BBO, we evaluate errors on inflationary parameters expected in these two future experiments. To calculate the Fisher matrices, we need to obtain differentiation of the spectrum with respect to the model parameters assuming a fiducial model. The CMB spectra are computed using the CAMB code [15]. For the gravitational wave spectra at direct detection scales, we present two different approaches: an analytical way with the slow-roll approximation and a numerical way. We first apply the Fisher matrix method to the slow-roll paradigm, which enables us to express the spectrum in terms of the parameters defined at the CMB scale. This slow-roll framework is a simple and well-established way to connect the amplitude of the spectrum at different scales. However, since this method uses the Taylor expansion to extend the spectrum from the CMB scale, the approximated spectrum may deviate slightly from the true value at the direct detection scale [16]. For this reason, we also present the case in which numerical calculations are used to obtain the precise amplitude of the spectrum. This method, however, requires us to assume an inflation model. Therefore, both of the methods have their advantages and disadvantages; the slow-roll paradigm can be applied as a more general model, which does not require us to assume an inflation model like the numerical method, while the numerical calculation enables us to make a more accurate prediction.

The outline of this paper is as follows: In Sec. II, we briefly introduce the Fisher matrix methods for both CMB measurements and direct detection of the gravitational wave background. In Sec. III, the Fisher method is applied to the slow-roll paradigm. We show how direct detection reduces errors obtained from CMB in the $n_S - r$ plane by connecting n_S and r with parameters of the gravitational wave spectrum assuming slow-roll inflation. In Sec. IV, the investigation with numerically calculated spectra is given for several inflation models which predict a large enough amplitude of the gravitational waves to be detected by BBO. We also allow the temperature of reheating to be a free parameter. We show to what extent potential parameters can be determined when the constraints from CMB and direct detection are combined. Conclusions are given in Sec. V.

TABLE I: Planck instrument characteristics

Center frequency (GHz)	70	100	143	217
θ (FWHM arcmin)	14	10	7.1	5.0
σ_T (μK)	12.8	6.8	6.0	13.1
σ_E (μK)	18.2	10.9	11.4	26.7
σ_B (μK)	18.2	10.9	11.4	26.7

II. FISHER MATRIX METHODS

The Fisher information matrix is commonly used in cosmology to predict how well parameters can be determined in future planned experiments, and is defined as the second derivative of the log likelihood function \mathcal{L} with respect to the model parameters p_i ,

$$\mathcal{F}_{ij} = - \left\langle \frac{\partial^2 \ln \mathcal{L}}{\partial p_i \partial p_j} \right\rangle. \quad (1)$$

According to the Cramer-Rao inequality, the Fisher matrix gives a lower bound for variances of the parameter estimates. This enables us to estimate expected errors on model parameters for a given experiment. The likelihood function is constructed from the specifications of each experiment.

A. CMB B -mode polarization

The CMB Fisher matrix is given by (see for example [17])

$$\mathcal{F}_{ij} = \sum_{\ell} \sum_{X, X'} \frac{\partial C_{\ell}^X}{\partial p_i} \text{Cov}^{-1}(C_{\ell}^X, C_{\ell}^{X'}) \frac{\partial C_{\ell}^{X'}}{\partial p_j}, \quad (2)$$

where X and X' are summed over the the CMB temperature, E -mode, and B -mode of the CMB polarization. The covariance matrix can be obtained from Zaldarriaga et. al. [17] and depends on the temperature noise per pixel (σ_T), the polarization noise per pixel (σ_E and σ_B), the pixel area in radians squared ($\theta^2 = 4\pi/N_{\text{pix}}$), and the beam window function which we approximate as Gaussian ($\mathcal{B}_{\ell} \approx \exp(-\ell(\ell+1)\sigma_b^2)$). The values we use are taken from the Planck blue book¹ and are listed in Table I (note that θ needs to be converted to radians). We use $\sigma_b = \theta/\sqrt{8 \ln 2}$ and combine the different frequency bands as specified in Bond et. al. [18]. We take the range in ℓ to be 2 to 2000. At higher ℓ , secondary sources of temperature and polarization will likely prohibit the extraction of cosmological information from the primary CMB. We assume that the foregrounds can be removed by using templates and multifrequency information; see, for example, Efstathiou *et al.* Efstathiou et.al. [19]. We also

¹ [http://www.rssd.esa.int/SA/PLANCK/docs/Bluebook-ESA-SCI\(2005\)1_V2.pdf](http://www.rssd.esa.int/SA/PLANCK/docs/Bluebook-ESA-SCI(2005)1_V2.pdf)

consider the case of a cosmic variance-limited (in both temperature and polarization) CMB experiment (CV) for $\ell \leq 2000$ and without delensing. This would be similar to optimistic foreground removal with epic-2m [20].

Throughout this paper, we assume a flat Λ cold dark matter Universe and we use the WMAP5 maximum likelihood values for the nonprimordial power spectrum parameters [21]: (baryon density) $\Omega_b h^2 = 0.0227$, (CDM density) $\Omega_c h^2 = 0.108$, (amplitude of curvature perturbations) $\Delta_{\zeta, \text{prim}}^2 = 2.41 \times 10^{-9}$, (reionization optical depth) $\tau = 0.089$, and (the Hubble parameter) $h = 0.724$.

B. Direct detection of gravitational waves

In a direct detection experiment, cross correlation analysis is a powerful method to detect a weak stochastic gravitational wave background, such as inflationary gravitational waves [22–25]. The Fisher information matrix for the cross correlation analysis is given as [26]

$$\mathcal{F}_{ij} = \left(\frac{3H_0^2}{10\pi^2} \right)^2 2T_{\text{obs}} \times \sum_{(I,J)} \int_0^\infty df \frac{|\gamma_{IJ}(f)|^2 \partial_{p_i} \Omega_{\text{GW}}(f) \partial_{p_j} \Omega_{\text{GW}}(f)}{f^6 S_I(f) S_J(f)}, \quad (3)$$

where f is the frequency of the gravitational waves, H_0 is the Hubble constant, T_{obs} is observation time. Here, we consider TDI (Time-Delay Interferometry) channel output ($I = A, E, T$) which would be adopted in the BBO project. In this case, the noise transfer functions $S_{A,E,T}(f)$ are given as [27, 28]

$$S_A(f) = S_E(f) = 8 \sin^2(\hat{f}/2) [(2 + \cos \hat{f}) S_n^p(f) + 2(3 + 2 \cos \hat{f} + \cos(2\hat{f})) S_n^a(f)], \quad (4)$$

$$S_T(f) = 2[1 + 2 \cos \hat{f}]^2 [S_n^p(f) + 4 \sin^2(\hat{f}/2) S_n^a(f)], \quad (5)$$

where $\hat{f} = 2\pi L f$ and L is the arm length of the detector which is assumed the same for each arm. In the case of the standard BBO detector, the arm length is $L = 5.0 \times 10^4 \text{ km}$ and noise functions are $S_n^p = 2.0 \times 10^{-34} / L^2 \text{ Hz}^{-1}$, $S_n^a = 9.0 \times 10^{-34} / (2\pi f)^4 / (2L)^2 \text{ Hz}^{-1}$.² The overlap reduction function $\gamma_{IJ}(f)$ is calculated with information about relative locations and orientations of detectors [30–32].

The intensity of a stochastic gravitational wave background is characterized by the dimensionless quantity

$$\Omega_{\text{GW}} \equiv \frac{1}{\rho_c} \frac{d\rho_{\text{GW}}}{d \ln k}, \quad (6)$$

where the wavenumber relates to the frequency as $k = 2\pi f$. The critical density of the Universe is defined as $\rho_c \equiv 3H^2/8\pi G$, where H is defined by the scale factor $a(t)$ as $H = \dot{a}/a$, and the energy density of the gravitational waves ρ_{GW} is given by the 00 component of the stress-energy tensor. Let us consider the tensor perturbation in a Friedmann-Robertson-Walker metric, $ds^2 = -dt^2 + a^2(t)(\delta_{ij} + h_{ij})dx^i dx^j$. It is convenient to expand h_{ij} into its Fourier components,

$$h_{ij}(t, \mathbf{x}) = \sum_{\lambda=+, \times} \int \frac{d^3 k}{(2\pi)^{3/2}} \epsilon_{ij}^\lambda(\mathbf{k}) h_{\mathbf{k}}^\lambda(t) e^{i\mathbf{k} \cdot \mathbf{x}}, \quad (7)$$

where the polarization tensors $\epsilon_{ij}^{+, \times}$ satisfy symmetric and transverse-traceless conditions and are normalized as $\sum_{i,j} \epsilon_{ij}^\lambda (\epsilon_{ij}^{\lambda'})^* = 2\delta^{\lambda\lambda'}$. Then ρ_{GW} is given as

$$\begin{aligned} \rho_{\text{GW}} &= \frac{1}{64\pi G} \langle (\partial_t h_{ij})^2 + \left(\frac{1}{a} \vec{\nabla} h_{ij}\right)^2 \rangle \\ &= \frac{1}{32\pi G} \int \frac{d^3 k}{(2\pi)^3} \frac{k^2}{a^2} 2 \sum_{\lambda} |h_{\mathbf{k}}^\lambda|^2, \end{aligned} \quad (8)$$

which yields

$$\Omega_{\text{GW}} = \frac{1}{12} \left(\frac{k}{aH} \right)^2 \frac{k^3}{\pi^2} \sum_{\lambda} |h_{\mathbf{k}}^\lambda|^2. \quad (9)$$

One may use the tensor power spectrum $\Delta_h^2(k)$ instead of Ω_{GW} , which is defined as

$$\Delta_h^2(k) \equiv \frac{d\langle h_{ij} h^{ij} \rangle}{d \ln k} = \frac{k^3}{\pi^2} \sum_{\lambda} |h_{\mathbf{k}}^\lambda|^2. \quad (10)$$

III. SLOW-ROLL PARADIGM

First, we present a Fisher matrix calculation making use of analytical models of slow-roll inflation. The basic assumption here is that inflation is driven by a slow-rolling single scalar field and the slow-roll approximation is valid while the scalar field rolls down the potential from the point which relates the CMB scale to the point of the direct detection scale.

A. Slow-roll prediction for the spectrum of the gravitational wave background

In an analytic approach, it is convenient to divide the spectrum of the gravitational wave background into two parts: the initial power spectrum $\Delta_{h, \text{prim}}^2$ and the transfer function T_h ,

$$\Omega_{\text{GW}} = \frac{1}{12} \left(\frac{k}{aH} \right)^2 \Delta_{h, \text{prim}}^2(k) T_h^2(k). \quad (11)$$

The initial power spectrum is predicted under the slow-roll approximation. In standard slow-roll inflation, a

² We have taken S_n^p to be 4 times larger than the contribution from photon shot noise alone, following Refs. [11, 29].

scalar field ϕ slowly rolls down its potential $V(\phi)$, and the equation of motion is given as $\ddot{\phi} + 3H\dot{\phi} + V'(\phi) = 0$, where the dot and prime denote the derivative with respect to t and ϕ respectively. We define the slow-roll parameters in terms of V and its derivatives,

$$\epsilon \equiv \frac{m_{\text{Pl}}^2}{16\pi} \left(\frac{V'}{V} \right)^2, \quad (12)$$

$$\eta \equiv \frac{m_{\text{Pl}}^2}{8\pi} \frac{V''}{V}, \quad (13)$$

where $m_{\text{Pl}} = 1/\sqrt{G}$ is the Planck mass. The initial power spectra of scalar and tensor perturbations are predicted as

$$\Delta_{\zeta, \text{prim}}^2(k) \simeq \frac{1}{\pi\epsilon} \left(\frac{H}{m_{\text{Pl}}} \right)^2 \Big|_{k=aH}, \quad (14)$$

$$\Delta_{h, \text{prim}}^2(k) \simeq \frac{16}{\pi} \left(\frac{H}{m_{\text{Pl}}} \right)^2 \Big|_{k=aH}, \quad (15)$$

which give the tensor-to-scalar ratio

$$r \equiv \frac{\Delta_{h, \text{prim}}^2(k)}{\Delta_{\zeta, \text{prim}}^2(k)} \simeq 16\epsilon. \quad (16)$$

One may define inflationary parameters at a pivot wavenumber k_0 and express the initial power spectrum in a Taylor-expanded form as [33, 34]

$$\ln \frac{\Delta_{h, \text{prim}}^2(k)}{\Delta_{h, \text{prim}}^2(k_0)} = n_T(k_0) \ln \frac{k}{k_0} + \frac{1}{2} \alpha_T(k_0) \ln^2 \frac{k}{k_0} + \dots, \quad (17)$$

where the tensor spectral index $n_T(k)$ and its running $\alpha_T(k)$ are given in terms of the slow-roll parameters

$$n_T(k) \equiv \frac{d \ln \Delta_{h, \text{prim}}^2(k)}{d \ln k} \simeq -2\epsilon, \quad (18)$$

$$\alpha_T(k) \equiv \frac{d n_T(k)}{d \ln k} \simeq 4\epsilon\eta - 8\epsilon^2. \quad (19)$$

Similarly, the scalar spectral index $n_S(k)$ and its running $\alpha_S(k)$ are given as

$$n_S(k) - 1 \equiv \frac{d \ln \Delta_{\zeta, \text{prim}}^2(k)}{d \ln k} \simeq -6\epsilon + 2\eta, \quad (20)$$

$$\alpha_S(k) \equiv \frac{d n_S(k)}{d \ln k} \simeq -16\epsilon\eta + 24\epsilon^2 + 2\xi^2, \quad (21)$$

where $\xi^2 \equiv (m_{\text{Pl}}/2\pi)^4 V'V'''/V^2$. Throughout this paper, we use parameter values evaluated at the CMB scale $k_0 = 0.002 \text{Mpc}^{-1}$. From Eqs. (16) and (18), we obtain a relation of single-field slow-roll inflation, which is called the consistency relation

$$r = -8n_T. \quad (22)$$

From the relations of the slow-roll prediction, the tensor mode parameters can be connected with the

other parameters as $n_T(k_0) \simeq -r/8$ and $\alpha_T(k_0) \simeq r/8(n_S + r/8 - 1)$. Therefore, in the framework of slow-roll inflation, the primordial spectrum can be written in terms of the parameters familiar in CMB observation, r , n_S and $\Delta_{\zeta, \text{prim}}^2$, as

$$\Delta_{h, \text{prim}}^2(k) = r \Delta_{\zeta, \text{prim}}^2 \times \exp \left[-\frac{r}{8} \ln \frac{k}{k_0} + \frac{r}{16} \left(n_S + \frac{r}{8} - 1 \right) \ln^2 \frac{k}{k_0} \right]. \quad (23)$$

The transfer function for the simple case where the components of the Universe are only radiation and matter is given in Ref. [35] as $T_h^2(k) = (3j_1(k\tau_0)/k\tau_0)^2 (1 + 1.34x_{\text{eq}} + 2.5x_{\text{eq}}^2)$, where $x_{\text{eq}} = k/k_{\text{eq}}$, $k_{\text{eq}} \equiv \tau_{\text{eq}}^{-1} = 6.22 \times 10^{-2} \Omega_m h^2 \text{Mpc}^{-1}$, and $\tau_0 = 2H_0^{-1}$. The spherical Bessel function, $j_1(x) = (\sin x - x \cos x)/x^2$, is replaced as $j_1(k\tau_0) \rightarrow 1/(\sqrt{2}k\tau_0)$ when taking the limit of $k\tau_0 \ll 1$ and averaging the oscillation. Additionally, the amplitude of the spectrum is suppressed by the cosmological constant [36] and changes in the effective degrees of freedom during the radiation-dominated era [37] at direct detection frequencies. A suppression factor due to the cosmological constant is $(1 - \Omega_\Lambda)^2$, explained in the Appendix. A damping factor due to the effective degrees of freedom is evaluated with the temperature when the corresponding mode enters the horizon, T_{hc} , as $(g_*(T_{\text{hc}})/g_{*0})(g_{*s0}/g_{*s}(T_{\text{hc}}))^{4/3}$, where $g_{*0} = 3.36$ and $g_{*s0} = 3.90$ [38]. In the case of taking into account only particles in the standard model and not including SUSY particles or any other exotic particles, the effective degrees of freedom which correspond to the direct detection scale are $g_*(T_{\text{hc}}) = g_{*s}(T_{\text{hc}}) = 106.75$. Adding these two factors to the transfer function of Ref. [35], we obtain [39]

$$T_h^2(k) = (1 - \Omega_\Lambda)^2 \left(\frac{g_*(T_{\text{hc}})}{g_{*0}} \right) \left(\frac{g_{*s0}}{g_{*s}(T_{\text{hc}})} \right)^{4/3} \left(\frac{3}{\sqrt{2}(k\tau_0)^2} \right)^2 (1 + 1.34x_{\text{eq}} + 2.5x_{\text{eq}}^2). \quad (24)$$

We use this transfer function for the spectrum at the direct detection scale, which is calculated by substituting Eqs. (23) and (24) into Eq. (11).

B. Errors on inflationary parameters

Using the analytic spectrum from the slow-roll approximation, we calculate the Fisher matrix and forecast errors on the parameters attainable from Planck and BBO. We take $(h, \Omega_b h^2, \Omega_c h^2, \tau, n_S, r, \Delta_{\zeta, \text{prim}}^2)$ as model parameters. Note that the direct detection is not sensitive to the values of $h, \Omega_b h^2, \Omega_c h^2, \tau$ at all. Although the transfer function given in Eq. (24) includes $h, \Omega_m h^2 (= \Omega_b h^2 + \Omega_c h^2)$ and $1 - \Omega_\Lambda (= \Omega_m)$, their effects cancel out when the transfer function is evaluated at higher frequencies ($k \gg k_{\text{eq}}$). So practically we take

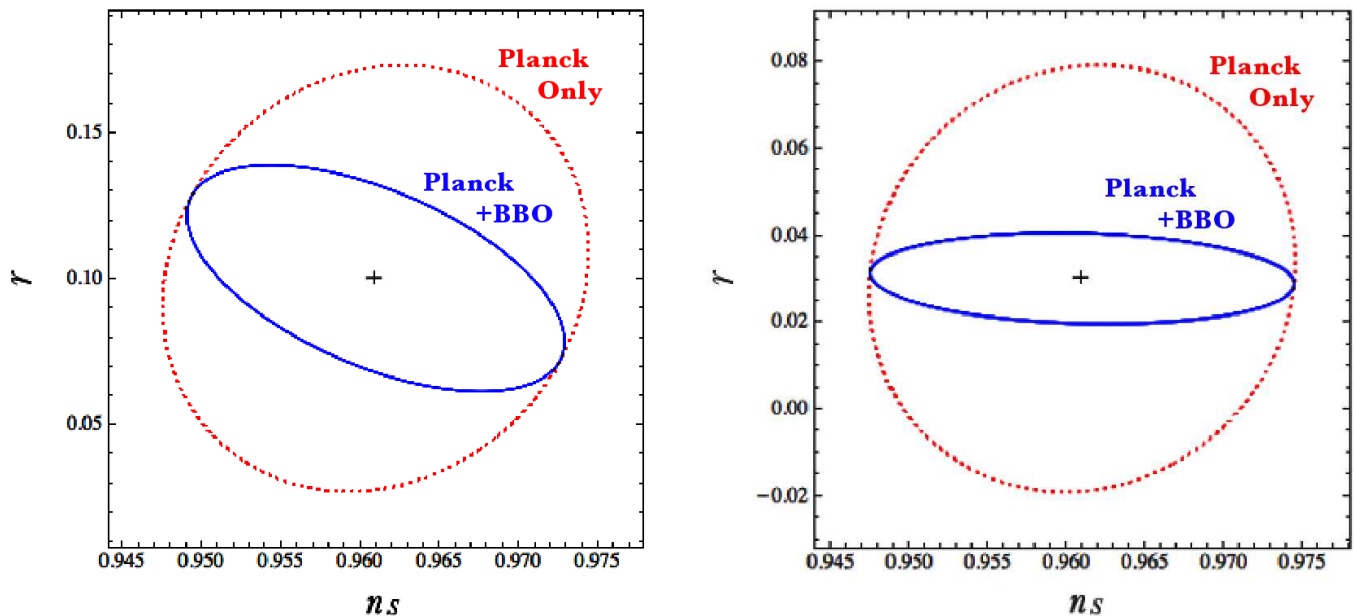


FIG. 1: Forecast constraints on n_S and r . The dotted line ellipse (red) represents the marginalized 2σ confidence level by Planck only, and the solid one (blue) represents combined constraints from Planck and BBO. The fiducial parameters are $r_{\text{fid}} = 0.1$ in the left panel, $r_{\text{fid}} = 0.03$ in the right panel.

ss

Variable	Fiducial value	% Error Planck only	% Error Planck+BBO	% Error CV	% Error CV+BBO
h	0.724	1.1	1.	0.11	0.11
$\Omega_c h^2$	0.108	1.3	1.2	0.15	0.15
$\Omega_b h^2$	0.227	0.88	0.83	0.13	0.13
τ	0.089	4.1	4.1	1.8	1.8
n_S	0.961	0.56	0.5	0.11	0.1
r	0.1	29.	16.	1.	1.
$\Delta_{\zeta, \text{prim}}^2$	2.41×10^9	0.79	0.77	0.29	0.29

Variable	Fiducial value	% Error Planck only	% Error Planck+BBO	% Error CV	% Error CV+BBO
h	0.724	1.1	1.1	0.1	0.1
$\Omega_c h^2$	0.108	1.3	1.3	0.15	0.15
$\Omega_b h^2$	0.227	0.88	0.88	0.13	0.13
τ	0.089	4.1	4.	1.7	1.7
n_S	0.961	0.57	0.57	0.1	0.1
r	0.03	66.	14.	1.6	1.6
$\Delta_{\zeta, \text{prim}}^2$	2.41×10^9	0.64	0.64	0.25	0.25

TABLE II: Marginalized 1σ (68%) errors on parameters for the slow-roll inflation model. The upper table is for the $r_{\text{fid}} = 0.1$ case; the lower table is for the $r_{\text{fid}} = 0.03$ case.

$(n_S, r, \Delta_{\zeta, \text{prim}}^2)$ as free parameters in the calculation of the Fisher matrix for direct detection. Here, we show two cases of different fiducial values of r : $r_{\text{fid}} = 0.1$ and 0.03 . The fiducial values of the other parameters are taken to be the WMAP5 maximum likelihood. We use Eq. (22) for n_T . The gravitational wave background has a direct detection with SNR=18.2 in the case of $r_{\text{fid}} = 0.1$, and SNR=8.9 in $r_{\text{fid}} = 0.03$.

Figure 1 shows the constraints in the $n_S - r$ plane expected from Planck, and those combined with constraints from 10 years of observation with BBO. The Planck con-

straints on n_S and r are not particularly degenerate as most of the constraint for r comes from the B -mode of the CMB polarization and most of the constraint for n_S comes from the temperature measurements. The degenerate direction of direct detection constraints is the direction along which the model gives the same amplitude of the gravitational wave background spectrum at the direct detection frequencies. Since direct detection detects gravitational waves with a very narrow bandwidth (0.1 – 1Hz), it has less sensitivity to the tilt of the spectrum by itself and cannot measure a small de-

viation from the scale-invariant spectrum. Considering the fact that direct detection is sensitive only for the amplitude of the spectrum, the degeneracy line is considered to be the direction of $\Delta\Omega_{\text{GW}}(f = 0.2\text{Hz}) = 0$. We can evaluate the degeneracy line in the $n_S - r$ plane assuming that $\Delta_{\zeta, \text{prim}}^2$ is fixed in Eq. (23), which yields $\Delta\Omega_{\text{GW}}(k) \propto \Delta(\Delta_{h, \text{prim}}^2) = [1 - r \ln(k/k_0)/8 + r(n_S + r/4 - 1) \ln^2(k/k_0)/16]\Delta r + r^2 \ln^2(k/k_0)\Delta n_S/16$. Substituting $k/k_0 \simeq 6.5 \times 10^{16}$ at $k = 2\pi \times 0.2\text{Hz}$, we infer that the error ellipse is elongated along the directions of $0.39\Delta r + 0.94\Delta n_S = 0$ for $r_{\text{fid}} = 0.1$, and $0.77\Delta r + 0.084\Delta n_S = 0$ for $r_{\text{fid}} = 0.03$. This is consistent with the direction of the main axis of the error ellipse for Planck+BBO shown in Fig. 1. Note that the error ellipses obtained by direct detection alone are much more elongated in these directions, but thanks to the tight constraint on n_S from CMB, the combined ellipses are less elongated. Also, the direct detection constraint itself has no power to distinguish r and $\Delta_{\zeta, \text{prim}}^2$ both of which strongly affect the amplitude of the spectrum [see Eq. (23)]. However, the CMB gives a quite tight constraint on $\Delta_{\zeta, \text{prim}}^2$ and the degeneracy in the direction of $\Delta_{\zeta, \text{prim}}^2$ is broken when they are combined.

As expected, we see direct detection has power mainly in determining the tensor-to-scalar ratio r to which CMB is not very sensitive. It is notable that direct detection tightens the constraint on r more in the case of $r_{\text{fid}} = 0.03$ as compared to $r_{\text{fid}} = 0.1$. This can be explained as follows: When n_S and $\Delta_{\zeta, \text{prim}}^2$ are fixed, Eq. (23) yields $\Delta\Omega_{\text{GW}}(k) \propto [1 - r \ln(k/k_0)/8 + r(n_S + r/4 - 1) \ln^2(k/k_0)/16]\Delta r$. Since the direct detection does not have sensitivity to the frequency dependence, it is reasonable to evaluate the uncertainty fixing the frequency at 0.2Hz as we did above. Then the errors on r are expected to be $\sigma_r \sim \Delta r \propto (1 - 8.5r + 23.4r^2)^{-1}$. This is an increasing function when $r \lesssim 0.18$, which means the error becomes smaller as r decreases. This happens because the amplitude is not sensitive to r around $r \sim 0.18$ due to the balance between the effect of r to increase the amplitude of the tensor-to-scalar ratio and the effect to decrease the amplitude via the tilt of the spectrum, $\exp(-r \ln(k/k_0)/8)$, as seen in Eq. (23). Therefore, $\Omega_{\text{GW}}(f = 0.2\text{Hz})$ changes more rapidly with the variation of r when r is smaller, and this results in the smaller error on r in the $r_{\text{fid}} = 0.03$ case. As r decreases more, σ_r goes to a constant value and direct detection no longer has power to determine r . In that case, BBO may give an upper limit $r \lesssim 0.008$ with a 3σ confidence level.

The errors on the other parameters are listed as percentages of the fiducial values in Table II. We see that direct detection does not help to improve the constraints on CV in this model.

IV. NUMERICAL CALCULATION

In this section, we perform the Fisher matrix calculation using the spectrum of the gravitational wave background which is obtained by numerically solving the evolution equation of the gravitational waves. We calculate the evolution of the scalar field numerically and follow the evolution of the gravitational waves from the inflation phase up to the present. This means the amplitude of the spectrum obtained numerically reflects the actual Hubble expansion rate when each mode exits the horizon during inflation. In contrast, the slow-roll prediction presented in the previous section may not predict the precise amplitude of the spectrum at scales far from the CMB scale, since the spectrum is expressed by making use of a Taylor series approximation. However, while this numerical approach has the advantage of allowing for precise evaluation of the amplitude, this numerical approach requires us to assume an inflation model. Here, we evaluate errors on each potential model parameter of quadratic inflation (one potential parameter case), and natural inflation (two potential parameter case), which can give a relatively large amplitude of the gravitational wave background.

A. Method

First, we briefly present the method of our numerical calculation (for details, see Ref. [16]). The evolution equation of the gravitational wave is simply expressed as

$$\ddot{h}_{\mathbf{k}}^\lambda + 3H\dot{h}_{\mathbf{k}}^\lambda + \frac{k^2}{a^2}h_{\mathbf{k}}^\lambda = 0. \quad (25)$$

We evolve this equation by calculating H numerically using the following equations. During inflation, the evolution of the Hubble expansion is determined by the scalar field, which decays into radiation in the reheating phase following inflation. When considering a case that the decay rate Γ is sufficiently small, the effect of decay can be simply included into the scalar field equation as [40, 41]

$$\ddot{\phi} + (3H + \Gamma)\dot{\phi} + V' = 0, \quad (26)$$

and the energy density of the radiation ρ_r generated from the scalar field obeys the equation,

$$\dot{\rho}_r + 4H\rho_r = \Gamma\rho_\phi. \quad (27)$$

Then the Hubble expansion is determined by the energy density of the ϕ field and radiation field,

$$H^2 = \frac{8\pi}{3m_{\text{Pl}}^2}(\rho_\phi + \rho_r), \quad (28)$$

where the energy density of this scalar field is given as $\rho_\phi = \dot{\phi}^2/2 + V$. After the Universe become well radiation dominated, we switch to the equation for the Hubble

expansion rate which takes into account the change of g_* ,

$$H^2 = H_0^2 \left[\left(\frac{g_*}{g_{*0}} \right) \left(\frac{g_{*s0}}{g_{*s}} \right)^{4/3} \Omega_r a^{-4} + \Omega_m a^{-3} + \Omega_\Lambda \right], \quad (29)$$

where we take $\Omega_r h^2 = 4.15 \times 10^{-5}$ and the other cosmological parameters are set to be the WMAP maximum likelihood values given in Sec. II A.

We derive the amplitude of the spectrum by solving the above equations numerically. The derivative of the spectrum, which is necessary for the Fisher calculation, is calculated by performing several calculations in which we change the parameters slightly. Here, not only do we take potential model parameters as parameters for the Fisher matrix, but we also take the number of e foldings \mathcal{N} as a parameter. The e -folding number is defined as $\mathcal{N}(k) \equiv \ln(a_{\text{end}}/a_k)$, where a_{end} is the scale factor at the end of inflation and a_k is the scale factor when the mode exit the horizon ($k = aH$) during inflation. When considering a mode which corresponds to the CMB scale $k_0 = 0.002 \text{Mpc}^{-1}$, the value of \mathcal{N} is approximately given as [42]

$$\mathcal{N} \simeq 56 - \frac{2}{3} \ln \frac{10^{16} \text{GeV}}{\rho_{\text{end}}^{1/4}} - \frac{1}{3} \ln \frac{10^9 \text{GeV}}{T_{\text{RH}}}, \quad (30)$$

where ρ_{end} is the energy density at the end of inflation and T_{RH} is the reheating temperature, which directly relates to the decay rate as [40]

$$T_{\text{RH}} \simeq g_*^{-(1/4)} \left(\frac{45}{8\pi^3} \right)^{1/4} (m_{\text{PI}} \Gamma)^{1/2}. \quad (31)$$

Note that we do not use Eq. (30) to obtain the fiducial value of \mathcal{N} , which is given numerically for a given value of Γ .

Here, we have assumed reheating to take place via perturbative decay [43, 44] as this process can be included simply as in Eqs. (26) and (27). However, in many cases there can be a stage of preheating (see for example [45, 46]) where the inflaton decays via parametric resonance. In this paper, we choose a low decay rate consistent with decay from gravitational effects [47] which results in a reheating temperature of about 10^9 GeV, and so in the inflation models we consider there will not be a preheating phase. This corresponds to taking $\Gamma \simeq 2 \text{GeV}$ in Eq. (31).

In order to evaluate the primordial power spectrum parameters, which is necessary to calculate the Fisher matrix of the CMB, we use the usual slow-roll formulas to evaluate the parameters given in Sec. III A, by evaluating them when the mode of k_{piv} exit the horizon $k = aH$ in the numerical calculation of the background equations. This method is reasonable since the slow-roll formulas are sufficiently accurate for the primordial power spectrum at the length scales probed by the CMB. In addition to the model parameters taken for the CMB Fisher matrix in the previous section ($h, \Omega_b h^2, \Omega_c h^2, \tau, n_S, r, \Delta_{\zeta, \text{prim}}^2$), we also include the running of the scalar spectrum index α_S .

B. Quadratic Inflation

First, we investigate the case of the quadratic potential,

$$V = \frac{1}{2} m^2 \phi^2. \quad (32)$$

We take two model parameters: the mass of the scalar field m and e -folds number \mathcal{N} , or reheating temperature $\log_{10}(T_{\text{RH}}/\text{GeV})$. The error in \mathcal{N} can be converted to the error in $\log_{10}(T_{\text{RH}}/\text{GeV})$ by Eq. (30) as $\sigma_{\mathcal{N}} = 0.77 \sigma_{\log_{10}(T_{\text{RH}}/\text{GeV})}$. The fiducial value of m is determined to satisfy the normalization of the scalar perturbations $\Delta_{\zeta, \text{prim}}^2 = 2.41 \times 10^{-9}$, and \mathcal{N} is determined by $T_{\text{RH}} = 10^9 \text{GeV}$. They are derived numerically as $(m, \mathcal{N}) = (1.66 \times 10^{13} \text{GeV}, 55.7)$. In this case, the gravitational wave background is detected with $\text{SNR} = 16.5$ by the direct detection experiment.

Figure 2 shows the confidence contours in the $m - \mathcal{N}$ plane, expected from Planck, BBO and both combined. We see Planck gives good constraints on the mass of the scalar field m , but has less power to determine the e -folds number \mathcal{N} . Although the BBO constraint is weaker than Planck, it can break the strong degeneracy in the parameters since the degenerate directions are slightly different, and improve the errors on both of the parameters. Table III shows how much the errors from Planck and CV decrease when they are combined with the constraints from BBO.

Reminding the reader that direct detection cannot distinguish models which give the same amplitude at the direct detection frequencies, the degenerate direction is considered to be the direction in which $\Omega_{\text{GW}} \propto \Delta_{h, \text{prim}}^2 \propto H^2|_{k=aH}$ is constant [see Eq. (15)]. Using the relations that the Hubble expansion rate during inflation is given as $H(k)^2 \propto V(k) = m^2 \phi(k)^2/2$, and $\phi(k)$ relates to the e -folding number as $\phi(k)^2 = 2\mathcal{N}(k) + 1$ in the case of the quadratic potential model, the parameters give the same spectrum amplitude in the direction of $m^2[2\mathcal{N}(k) + 1] = \text{const}$. Therefore, the degenerate line is considered to be $\Delta m/m + \Delta \mathcal{N}/[2\mathcal{N}(k) + 1] = 0$. Substituting $\mathcal{N}(k = 2\pi \times 0.2 \text{Hz}) \simeq 16.4$ which corresponds to the direct detection scale, the degeneracy direction of the direct detection constraint is estimated as $\Delta m/(1.66 \times 10^{13} \text{GeV}) + \Delta \mathcal{N}/33.7 \simeq 0$, which is consistent with the result shown in Fig. 2.

We also show the constraints in terms of $\log_{10}(T_{\text{RH}}/\text{GeV})$ instead of \mathcal{N} . It is notable that the marginalized error on the reheating temperature is $\sigma_{\log_{10}(T_{\text{RH}}/\text{GeV})} \sim 6.0$ by Planck alone, which means the BBN lower limit of $\log_{10}(T_{\text{RH}}/\text{GeV}) = -3$ is less than 2σ away from the fiducial value without the direct detection constraint. When it is combined with direct detection constraint, the error is reduced to be $\sigma_{\log_{10}(T_{\text{RH}}/\text{GeV})} \sim 2.8$, and the BBN limit is ruled out at more than 4σ .

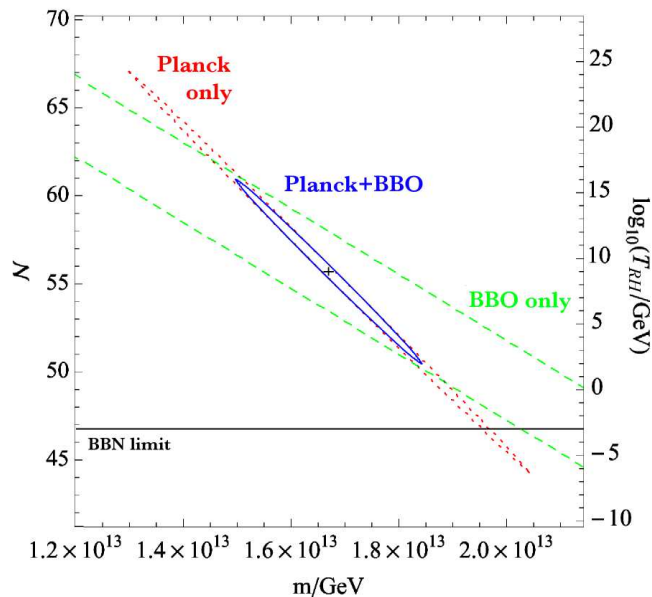


FIG. 2: Constraint on parameters of the quadratic potential. The dotted line (red) and the dashed line (green) show marginalized 2σ confidence region in the $m - \mathcal{N}$, $\log_{10} T_{\text{RH}}$ plane allowed by Planck and BBO, respectively, and the solid line (blue) shows the combined constraint. The black horizontal line shows the BBN limit on reheating temperature, $T_{\text{RH}} > 1\text{MeV}$.

Variable	Fiducial value	% Error Planck only	% Error Planck+BBO	% Error CV	% Error CV+BBO
h	0.724	0.64	0.49	0.15	0.15
$\Omega_c h^2$	0.108	0.84	0.62	0.2	0.2
$\Omega_b h^2$	0.227	0.52	0.5	0.17	0.17
τ	0.089	3.9	3.7	2.4	2.4
m/GeV	1.66×10^{13}	8.8	4.2	1.2	1.1
\mathcal{N}	55.7	8.3	3.9	1.1	1.1
$\log_{10}(T_{\text{RH}}/\text{GeV})$	9.0	67.	31.	9.1	8.8

TABLE III: Marginalized 1σ errors on parameters for the quadratic inflation model.

C. Natural inflation

Next, we investigate natural inflation for which the potential is given as [48–50]

$$V = \Lambda^4 \left[1 \pm \cos \left(\frac{N\phi}{f} \right) \right]. \quad (33)$$

Here, we set $N = 1$ and take the positive sign. In this case, we take three variables, Λ/m_{Pl} , f/m_{Pl} and \mathcal{N} , to be model parameters. We investigate two cases of different fiducial values of f , which are taken to be $f = m_{\text{Pl}}$ and $f = 2m_{\text{Pl}}$, and the fiducial value of Λ is determined by the normalization of $\Delta_{\zeta, \text{prim}}^2$. The potential becomes more quadratic and predicts larger amplitudes of the gravitational wave background as f increases. The fiducial values are, respectively, $(\Lambda/m_{\text{Pl}}, f/m_{\text{Pl}}, \mathcal{N}) = (1.07 \times 10^{-3}, 1.0, 55.2)$ for $f = m_{\text{Pl}}$ and $(1.64 \times 10^{-3}, 2.0, 55.6)$ for $f = 2m_{\text{Pl}}$. The gravitational wave background is detected with $\text{SNR} = 8.4$ in the case of $f = m_{\text{Pl}}$, and $\text{SNR} = 14.9$ in the case of $f = 2m_{\text{Pl}}$.

Figure 3 shows the error ellipsoids in the $f = 2m_{\text{Pl}}$

case. Table IV gives errors on each parameters. The $f = 2m_{\text{Pl}}$ case is essentially the quadratic case and so the errors on \mathcal{N} are about the same. A Taylor expansion around the bottom of the potential gives the effective mass to be $m \approx \Lambda^2/f$ when $f \gg 1$. Therefore the Λ and f parameters are expected to become correlated in the $f = 2m_{\text{Pl}}$ case and less so in the $f = m_{\text{Pl}}$ case. This is consistent with the errors of f and Λ being larger in the $f = 2m_{\text{Pl}}$ case. The gravitational waves are too low for the direct detection experiment to have much effect in the $f = m_{\text{Pl}}$ case. The error in the reheating temperature is quite large. Even in the $f = 2m_{\text{Pl}}$ case the Planck and direct detection data still has a fiducial value $T_{\text{RH}} = 10^9 \text{GeV}$ less than 3σ away from the BBN limit of $T_{\text{RH}} = 10^{-3} \text{GeV}$. Unlike in the quadratic inflation case, direct detection is still useful to tighten the constraints from CV for the $f = 2m_{\text{Pl}}$ model.

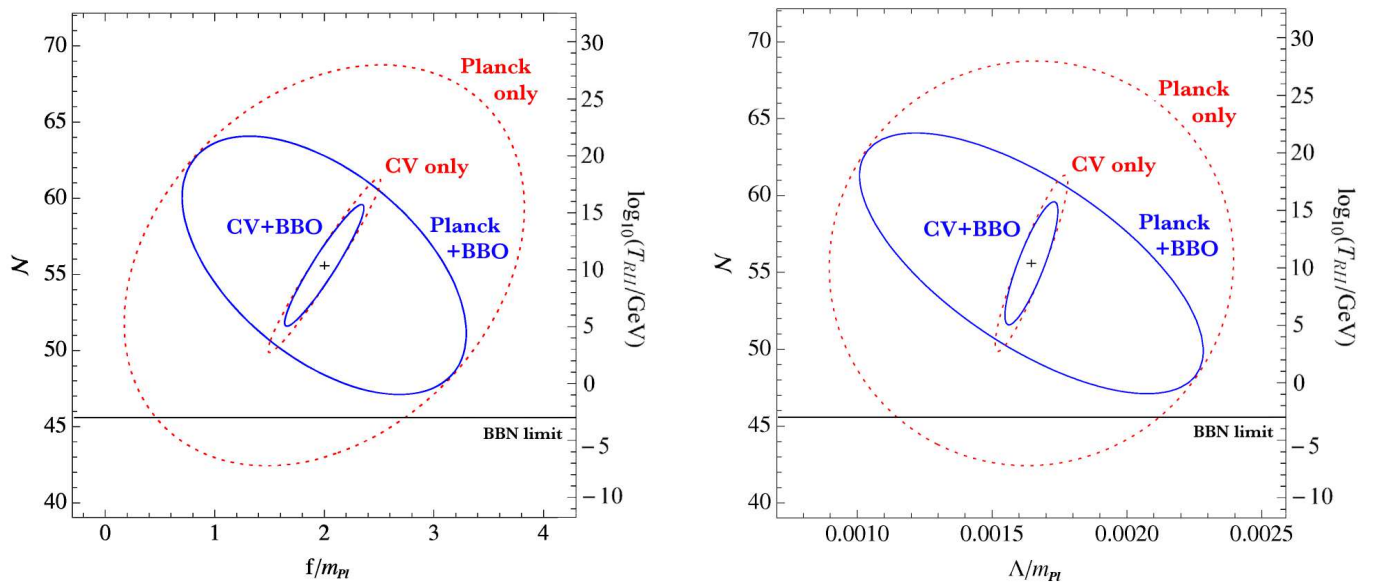


FIG. 3: Forecasted marginalized 2σ constraints on parameters for the natural inflation model with $f = 2m_{\text{Pl}}$. CMB (red dotted) and CMB plus direct detection (blue solid) are shown in the $f/m_{\text{Pl}} - \mathcal{N}$ and $\Lambda/m_{\text{Pl}} - \mathcal{N}$ plane, respectively. In each case the larger contour is when the CMB is Planck and the smaller is when the CMB is cosmic variance limited.

Variable	Fiducial value	% Error Planck only	% Error Planck+BBO	% Error CV	% Error CV+BBO
h	0.724	0.7	0.66	0.15	0.15
$\Omega_c h^2$	0.108	0.92	0.86	0.21	0.21
$\Omega_b h^2$	0.227	0.54	0.53	0.18	0.18
τ	0.089	3.7	3.7	2.4	2.4
Λ/m_{Pl}	1.07×10^{-3}	8.8	7.5	0.57	0.56
f/m_{Pl}	1.0	5.5	4.3	2.1	2.
\mathcal{N}	55.2	11.	10.	2.3	2.2
$\log_{10}(T_{\text{RH}}/\text{GeV})$	9.0	85.	83.	18.	18.

Variable	Fiducial value	% Error Planck only	% Error Planck+BBO	% Error CV	% Error CV+BBO
h	0.724	0.69	0.52	0.15	0.15
$\Omega_c h^2$	0.108	0.91	0.66	0.22	0.21
$\Omega_b h^2$	0.227	0.53	0.5	0.19	0.18
τ	0.089	3.9	3.8	2.6	2.4
Λ/m_{Pl}	1.64×10^{-3}	18.	16.	3.3	2.4
f/m_{Pl}	2.0	37.	26.	10.	7.3
\mathcal{N}	55.6	9.5	6.1	4.1	2.9
$\log_{10}(T_{\text{RH}}/\text{GeV})$	9.0	77.	49.	33.	23.

TABLE IV: Marginalized 1σ errors on parameters for the natural inflation model. The upper table is for the $f = m_{\text{Pl}}$ case; the lower table is for the $f = 2m_{\text{Pl}}$ case.

V. CONCLUSION

This paper is aimed at studying how direct detection of the inflationary gravitational wave background will determine inflationary parameters and how it will complement future CMB polarization experiments. An attractive feature of these two different methods of observation is that they probe two different frequencies and provide independent information. By calculating the Fisher matrix,

we have investigated the degree to which the errors on model parameters obtained from CMB experiments will be reduced by direct detection of the gravitational waves in the BBO experiment. We have presented two different types of methods to calculate the Fisher matrix: One is evaluated analytically by making use of the slow-roll approximation, and the other is evaluated numerically for the sake of more accurate predictions. In the second case, we also allow the temperature of reheating to be a free parameter.

In both cases, we have shown that the two different observations have different directions of parameter degeneracy and that this degeneracy is broken when they are combined. The degeneracy of a direct detection experiment is directed to the direction in which the model parameters give the same amplitude at the direct detection frequencies. Although our result indicates that the BBO experiment provides a larger error in parameter estimation than CMB experiments, it most certainly has the power to tighten constraints from Planck. We also found that for natural inflation, direct detection could even help to improve a cosmic variance-limited CMB experiment. It would be interesting to check what the improvements could be in multifield inflation models where the number of parameters would be greater.

Constraints on parameters which are defined by the slow-roll parameters were calculated by using an analytic spectrum of the gravitational wave background. BBO direct detection worked to tighten the constraint from Planck mainly on the tensor-to-scalar ratio. On the other hand, we have confirmed the intuitive fact that it does not have the power to constrain the other cosmological parameters, which makes sense since the tensor-to-scalar ratio is the major parameter in determining the amplitude of the gravitational wave background. Constraints on inflation potential parameters have been evaluated by using an accurate amplitude of the spectrum obtained from numerical calculations, for both the quadratic inflation and natural inflation cases. In addition to potential parameters, we also have taken the e -folds number, which corresponds to the reheating temperature, as a parameter and have found that BBO direct detection has power to tighten constraints on both of the parameters. For quadratic inflation, we found without BBO direct detection, Planck could only rule out a BBN reheating temperature at the 2σ level. However with BBO direct detection it could rule this out at almost the 4σ level. In the case of natural inflation (with $f = 2m_{\text{Pl}}$), we found that a cosmic variance-limited CMB experiment could only rule out a BBN reheating temperature at the 4σ level while with BBO direct detection it could be ruled out at almost the 6σ level.

Note that, when the signal to noise ratio is low, the Fisher matrix can underestimate the error bars (see for example [51]). Therefore our Planck only results may be overly optimistic, but the combined Planck plus BBO and the cosmic variance CMB results should be more accurate. In future work, we plan to redo this analysis using a Markov Chain Monte Carlo method, which will also make it easier to add more detailed priors on the reheating temperature.

For reference, let us mention another project aimed at detecting the inflationary gravitational wave background directly, called DECIGO [10]. It has similar specifications to BBO; the target frequency is almost the same, but the sensitivity is a little smaller than that of BBO. Because of the fact that the direction of the parameter degeneracy is determined only by the amplitude of the

gravitational wave at direct the detection scale, the degenerate direction of constraints from DECIGO is the same as the one from BBO. However, since DECIGO has less sensitivity, the size of the error ellipse is considered to be bigger than BBO and the Fisher matrix analysis may not be applicable unless the tensor-to-scalar ratio is relatively large. (For example, while BBO detects the gravitational wave background of $r = 0.1$ with $\text{SNR} = 18.2$, DECIGO detects this with $\text{SNR} = 4.1$, which may be out of the validity of the Fisher matrix analysis.) For this reason, we have presented the results only for BBO in this paper.

Acknowledgments

The authors are grateful to Kavilan Moodley and Naoki Seto for useful comments. SK would like to thank Tsutomu Takeuchi for his help with the study on the Fisher matrix analysis. This research is supported by Grant-in-Aid for Nagoya University Global COE Program, "Quest for Fundamental Principles in the Universe: From Particles to the Solar System and the Cosmos." CG is supported by the Becroft Institute for Particle Astrophysics and Cosmology.

Appendix A: Suppression factor for the cosmological constant

Reference [36] shows that the current acceleration of the Universe suppresses the amplitude of the inflation-produced gravitational waves by a factor of Ω_m/Ω_Λ . This is derived using the fact that the scale factor when the mode enter the horizon during the accelerating stage satisfies the relation $a_{\text{hc}} \propto k$. However, it is not appropriate to apply this to the case of our Universe, $\Omega_\Lambda = 0.7, \Omega_m = 0.3$, which just starts to enter the cosmological constant-dominated Universe and is still not in the middle of a de Sitter phase of exponential expansion.

Here, we propose a new suppression factor which gives a better approximation. From the behavior of the inflationary gravitational waves that $h_{\mathbf{k}}$ keeps constant outside the horizon and decreases proportional to a^{-1} after entering the horizon, the transfer function is considered to be written as $T_h(k) = |h_{\mathbf{k},0}|/|h_{\mathbf{k},\text{hc}}| = a_{\text{hc}}/a_0$. The suppression factor is measured by comparing the transfer functions in the case of the Universe without the cosmological constant, which we label with a subscript 1, and in the case with the cosmological constant, which we label with a subscript 2. Therefore, the value of interest, how much the amplitude of the gravitational waves is suppressed by the cosmological constant, is

$$\frac{T_{h,2}(k)}{T_{h,1}(k)} = \frac{a_{\text{hc},2}}{a_{\text{hc},1}}. \quad (\text{A1})$$

We set the Hubble parameter H_0 and the density parameter of radiation Ω_r to be the same value in both cases.

The only difference is the existence of the cosmological constant, Ω_Λ . If we assume a flat Universe, then the density parameter of matter is described with the amount of the cosmological constant as $\Omega_{m,2} = 1 - \Omega_r - \Omega_\Lambda$, while $\Omega_{m,1} = 1 - \Omega_r$ if there is no cosmological constant. With using the relation $k = a_{\text{hc}} H_{\text{hc}}$ and rewriting the Hubble parameter in terms of the cosmological parameters, Eq. (A1) becomes

$$\begin{aligned} \frac{a_{\text{hc},2}}{a_{\text{hc},1}} &= \frac{k/H_{\text{hc},2}}{k/H_{\text{hc},1}} \\ &= \frac{H_0 \sqrt{(1 - \Omega_r) a_{\text{hc},1}^{-3} + \Omega_r a_{\text{hc},1}^{-4}}}{H_0 \sqrt{(1 - \Omega_r - \Omega_\Lambda) a_{\text{hc},2}^{-3} + \Omega_r a_{\text{hc},2}^{-4} + \Omega_\Lambda}}. \end{aligned} \quad (\text{A2})$$

Let us consider a mode which enters the horizon dur-

ing the matter-dominated phase. Since the contribution of radiation and the cosmological constant terms to the Hubble expansion is negligible during this phase, Eq. (A2) becomes

$$\frac{a_{\text{hc},2}}{a_{\text{hc},1}} \simeq \sqrt{\frac{(1 - \Omega_r)}{(1 - \Omega_r - \Omega_\Lambda)} \left(\frac{a_{\text{hc},1}}{a_{\text{hc},2}}\right)^{-3}}}. \quad (\text{A3})$$

Neglecting the radiation density parameter, which is much smaller than 1, we find the suppression factor is approximately

$$\frac{a_{\text{hc},2}}{a_{\text{hc},1}} \simeq 1 - \Omega_\Lambda. \quad (\text{A4})$$

-
- [1] A. H. Guth, Phys. Rev. D **23**, 347 (1981).
[2] A. Albrecht and P. J. Steinhardt, Phys. Rev. Lett. **48**, 1220 (1982).
[3] A. Linde, Phys. Lett. B **108**, 389 (1982).
[4] B. Allen, Phys. Rev. D **37**, 2078 (1988).
[5] V. Sahni, Phys. Rev. D **42**, 453 (1990).
[6] L. P. Grishchuk and Y. V. Sidorov, Phys. Rev. D **42**, 3413 (1990); L. P. Grishchuk and M. Solokhin, Phys. Rev. D **43**, 2566 (1991).
[7] U. Seljak and M. Zaldarriaga, Phys. Rev. Lett. **78**, 2054 (1997); M. Zaldarriaga and U. Seljak, Phys. Rev. D **55**, 1830 (1997).
[8] M. Kamionkowski, A. Kosowsky, and A. Stebbins, Phys. Rev. Lett. **78**, 2058 (1997); Phys. Rev. D **55**, 7368 (1997).
[9] <http://www.rssd.esa.int/index.php?project=PLANCK>.
[10] N. Seto, S. Kawamura, and T. Nakamura, Phys. Rev. Lett. **87**, 221103 (2001); S. Kawamura *et al.*, Class. Quant. Grav. **23**, S125 (2006).
[11] E. S. Phinney *et al.*, "The Big Bang Observer", NASA Mission Concept Study (2003); G. M. Harry, P. Fritschel, D. A. Shaddock, W. Folkner and E. S. Phinney, Class. Quant. Grav. **23**, 4887 (2006) [Erratum-ibid. **23**, 7361 (2006)].
[12] T. L. Smith, M. Kamionkowski and A. Cooray, Phys. Rev. D **73**, 023504 (2006); Phys. Rev. D **78**, 083525 (2008).
[13] T. L. Smith, H. V. Peiris, and A. Cooray, Phys. Rev. D **73**, 123503 (2006).
[14] C. Ungarelli *et al.*, Classical Quantum Gravity **22**, 955 (2005).
[15] A. Lewis, A. Challinor, and A. Lasenby, Astrophys. J. **538**, 473 (2000).
[16] S. Kuroyanagi, T. Chiba and N. Sugiyama, Phys. Rev. D **79**, 103501 (2009).
[17] M. Zaldarriaga, D. Spergel, U. Seljak, Astrophys. J. **488** 1 (1997).
[18] J. R. Bond, G. Efstathiou and M. Tegmark, Mon. Not. R. Astron. Soc. **291**, L33 (1997).
[19] G. Efstathiou, S. Gratton and F. Paci, Mon. Not. R. Astron. Soc. **397**, 1355 (2009).
[20] D. Baumann *et al.*, arXiv:0811.3919 [astro-ph].
[21] J. Dunkley *et al.*, Astrophys. J. Suppl. **180** 306 (2009).
[22] P. F. Michelson, Mon. Not. R. Astron. Soc. **227**, 933 (1987).
[23] N. Christensen, Phys. Rev. D **46**, 5250 (1992).
[24] E. E. Flanagan, Phys. Rev. D **48**, 2389 (1993).
[25] B. Allen and J. D. Romano, Phys. Rev. D **59**, 102001 (1999).
[26] N. Seto, Phys. Rev. D **73**, 063001 (2006).
[27] T. A. Prince, M. Tinto, S. L. Larson, and J. W. Armstrong, Phys. Rev. D **66**, 122002 (2002).
[28] P. Bender *et al.*, "LISA Pre-Phase A Report", second Edition, MPQ 233, (1998); <http://lisa.gsfc.nasa.gov/Documentation/ppa2.08.pdf>
[29] C. Cutler and J. Harms, Phys. Rev. D **73**, 042001 (2006).
[30] N. J. Cornish and S. L. Larson, Classical Quantum Gravity **18**, 3473 (2001).
[31] N. J. Cornish, Phys. Rev. D **65**, 022004 (2001).
[32] V. Corbin and N. Cornish, Classical Quantum Gravity **23**, 2435 (2006).
[33] J. E. Lidsey *et al.*, Rev. Mod. Phys. **69**, 373 (1997).
[34] A. Kosowsky and M. S. Turner, Phys. Rev. D **52**, R1739 (1995).
[35] M. S. Turner, M. White and J. E. Lidsey, Phys. Rev. D **48**, 4613 (1993); M. S. Turner, Phys. Rev. D **55**, R435 (1997).
[36] Y. Zhang, Y. Yuan, W. Zhao and Y. T. Chen, Classical Quantum Gravity **22**, 1383 (2005).
[37] D. J. Schwarz, Mod. Phys. Lett. A **13**, 2771 (1998).
[38] Y. Watanabe and E. Komatsu, Phys. Rev. D **73**, 123515 (2006).
[39] K. Nakayama, S. Saito, Y. Suwa and J. Yokoyama, Phys. Rev. D **77**, 124001 (2008); J. Cosmol. Astropart. Phys. **06** (2008) 020.
[40] E. W. Kolb and M. S. Turner, *The Early Universe* (Westview Press, Boulder, CO, 1990).
[41] L. Kofman, A. Linde and A. A. Starobinsky, Phys. Rev. D **56**, 3258 (1997).
[42] D. H. Lyth and A. R. Liddle, *The Primordial Density Perturbation* (Cambridge University Press, 2009).
[43] A. D. Dolgov and A. D. Linde, Phys. Lett. B **116**, 329 (1982).
[44] L. F. Abbott, E. Farhi and M. B. Wise, Phys. Lett. B **117**, 29 (1982).

- [45] L. Kofman, A. D. Linde and A. A. Starobinsky, Phys. Rev. Lett. **76**, 1011 (1996).
- [46] P. B. Greene and L. Kofman, Phys. Rev. D **62**, 123516 (2000).
- [47] D. V. Nanopoulos, K. A. Olive and M. Srednicki, Phys. Lett. B **127**, 30 (1983).
- [48] K. Freese, J. A. Frieman and A. V. Olinto, Phys. Rev. Lett. **65**, 3233 (1990).
- [49] F. C. Adams, J. R. Bond, K. Freese, J. A. Frieman and A. V. Olinto, Phys. Rev. D **47**, 426 (1993).
- [50] C. Savage, K. Freese and W. H. Kinney, Phys. Rev. D **74**, 123511 (2006).
- [51] M. Vallisneri, Phys. Rev. D **77**, 042001 (2008).